Journal Pre-proof

Swelling-induced telephone cord blisters in hydrogel films

Bo Yuan, Christopher M. Harvey, Ke Shen, Rachel Thomson,
Gary Critchlow, David Rickerby, Suyuan Yu, Simon Wang

PII: S0263-8223(21)01343-X
DOI: https://doi.org/10.1016/j.compstruct.2021.114909
Reference: COST 114909

To appear in: *Composite Structures*

Received date : 12 August 2021
Revised date : 25 October 2021
Accepted date : 26 October 2021

Please cite this article as: B. Yuan, C.M. Harvey, K. Shen et al., Swelling-induced telephone cord blisters in hydrogel films. *Composite Structures* (2021), doi: https://doi.org/10.1016/j.compstruct.2021.114909.

Composite Structures, Volume 280, January 2022, Article number 114909
DOI:10.1016/j.compstruct.2021.114909

Swelling-induced telephone cord blisters in hydrogel films

Bo Yuan[a,*], Christopher M. Harvey[b,f], Ke Shen[c], Rachel Thomson[d], Gary Critchlow[d], David Rickerby[e], Suyuan Yu[a], Simon Wang[b,f,*]

[a]*Center for Combustion Energy, Department of Energy and Power Engineering, Tsinghua University,Beijing 100084, China*
[b]*Department of Aeronautical and Automotive Engineering, Loughborough University, Loughborough, Leicestershire LE11 3TU, UK*
[c]*Hunan Province Key Laboratory for Advanced Carbon Materials and Applied Technology, College of Materials Science and Engineering, Hunan University, Changsha, Hunan 410082, China*
[d]*Department of Materials, Loughborough University, Loughborough, Leicestershire LE11 3TU, UK*
[e]*Surface Engineering Precision Institute, Cranfield University, Cranfield, Bedfordshire MK43 0AL, UK*
[f]*School of Machinery and Equipment Engineering, Hebei University of Engineering, Handan 056038, China*

Abstract

Polymeric hydrogels can undergo dramatic shape and volumetric change when immersed into an appropriate solvent due to swelling or shrinking. Experimental studies have observed a variety of instability patterns in hydrogels. The telephone cord blister (TCB) with large deformability is one intriguing instability pattern but the assessment of its global morphology parameters, that is, the wavelength and transverse amplitude are still of inadequate appreciation. The present paper considers swelling-induced TCBs in a hydrogel-based film on a rigid substrate. Based on a previously developed theoretical framework for TCBs under small deformation, typically in a hard thin film, the theoretical derivations for the two global morphological parameters are furthermore developed for TCBs under large deformation in a soft thin film. Predictions for the morphology parameters of the developed theory agree very well with extensive experimental results. The critical mechanical conditions associated with the material-specific parameters such as the cross-linking density and swelling ratio are revealed. In addition, by reversing the calculation, the swelling-induced compressive stress in the un-delaminated film and the interfacial adhesion toughness are also accurately determined from measurements of the hydrogel TCBs. The present work provides an insight to design the microfluidics by controlling the morphology parameters with high precision.

Key words: Telephone cord blister, Compressive stress, Adhesion toughness, Hydrogel, Swelling, Buckling

*Corresponding author
Email addresses: Yuanbo11@mail.tsinghua.edu.cn (Bo Yuan), S.wang@lboro.ac.uk (Simon Wang)

Nomenclature

Λ	linear swelling ratio of hydrogel
λ	wavelength of blister under small deformation condition
ν	Poisson's ratio of film
σ_0	swelling-induced compressive stress in film
$\tilde{\lambda}$	wavelength of blister under large deformation condition
$\tilde{A}_y$	transverse amplitude of blister under large deformation condition
A_x	height of blister
A_y	transverse amplitude of blister under small deformation condition
E	Young's modulus of film
G_c	interface adhesion toughness of film/substrate material system
h	thickness of film
R	half-width that is perpendicular to the sinusoidal centreline of blister

1. Introduction

Thin films with thick substrates composites systems are ubiquitous in modern daily life and scientific and engineering applications. The films are in either hard or soft form depending on individual situations, and blisters of various morphologies can be formed in these films either on purpose or occurring as a damage. Therefore, it is of great value to have a better understanding of blisters formation mechanics and a capability for predicting their morphologies. For hard films, the generation and development of blisters are deemed to be undesirable as the function of the structural component will be lost. For instance, if blisters and spallation failure occur in thermal barrier coating material systems, the underneath metallic substrate will be exposed to the high-temperature and corrosion environment, leading to the loss of metals [1, 2]. In contrast, three-dimensional (3D) bioinspired configurations in soft materials are however desirable in the fields of Tissue Engineering [3], Biomedical Engineering [4], *etc.* since the highly deformable morphologies offer opportunities for novel designs, for instance, soft microfluidic control systems and soft biomimetic robotics that are inspired by the water circulation of mimosa leaves [5]. The large morphological deformation in a homogeneous soft film can be created in response to a small change in environmental stimulus, but not limited to temperature, pH value, light, ionic strength, *etc.* [6]. Moreover, by aligning anisotropic additions, composite soft materials exhibiting anisotropic swelling or inhomogeneous stimuli-response are used in the design of soft sensors or actuators [7–10].

The deformation of blisters and their morphologies are often related to deformation instability. A variety of deformation instability patterns have been identified in experimental studies [11–16] including wrinkles, creases, folds, ridges, *etc.* for both hard and soft thin films subjected to geometric confinement or mechanical loadings. From a conventional mechanical viewpoint, such structural instability patterns are caused by buckling or post-buckling that is driven by initial compressive stresses in the films before de-bonding at the interface. For hard film systems, the compressive stresses are usually led by mismatch strains between the dissimilar materials; however, for the soft materials such as a cross-linked polymer network film, when immersed in an appropriate solvent swelling occurs due to diffusion of the solvent. This in turn brings about large volumetric growth and compressive stresses in the soft material. For the buckling-driven delamination, an initial interface separation of critical size is required for given compressive stresses [17, 18]. Several studies [19–21] have proposed methods to design and fabricate deformable patterns with special considerations given to modifying the film thickness, the chemical composition such as the cross-linking density, the surface bonding geometry, the localised adhesion, the swelling degree, and the environmental sensitivity.

Takahashi *et al.* [20] created some distinctive 3D architectures in hydrogel-based thin films immersed in deionised water by processing selective adhesiveness at the interface. It was experimentally observed that a straight-sided blister was formed and developed at first during swelling in deionised water. After 170 s, it transformed to a TCB that propagated forward with wavy boundaries between the hydrogel film and the substrate. The TCB reached equilibrium in 600 s with progressive interface delamination and exhibited a large transverse amplitude-to-wavelength ratio which manifests deep post-secondary-buckling with large geometrical nonlinearity. The single-layer hydrogel film was furthermore covered with less-swellable bulk gels, creating a stacked hydrogel composite device. The stacked bulk gel acts as not only reinforcement matrix that stabilizes the microchannel architecture even at high flow rates for a long duration, but also a diffusive matrix that cultures cells [21].

Although Takahashi *et al.* [20, 21] performed systematic research to identify the parameters determining the formation and development of 3D architectures, quantitative analysis upon the correlations with the film thickness, cross-linking density, swelling ratio, and the geometry of the non-adhesive interface is still required for the design of microfluidic devices via artificially controlling the morphology parameters. Particularly, when the critical condition for conventional buckling is not satisfied, *i.e.*, the magnitude of swelling-induced compressive stress is smaller than the critical value, or alternatively the width of the non-adhesive region at the interface is small, the 'Ω-formulae' for the TCB in equilibrium developed by Yuan *et al.* [22] can be used to quantify the morphology parameters. It is noted that the Ω-formulae are based on a novel mechanical hypothesis originally proposed in Refs. [23, 24], that is, the delamination is driven by pockets of energy concentration. For the highly deformable and flexible soft hydrogel film, it is identified that the Ω-formulae for thin TCBs with small transverse amplitude-to-wavelength ratios still give accurate predictions for the two local morphology parameters, that is, the height and width; however, they are unable to give accurate predictions of the two global morphology parameters, that is, the wavelength and transverse amplitude. It is therefore necessary to furthermore develop the analytical Ω-formulae for TCBs with large deformability in soft thin films.

Based on the analytical mechanical models for the instability patterns in soft and

wet materials, the morphology-oriented design would be with higher precision by programming the associated physical parameters, and more importantly, it would provide theoretical tools for the determination of the swelling-induced stress and interface adhesion toughness of soft thin films through blister test [25, 26].

The present study aims to apply and develop the mechanical model proposed in Ref. [22] for the morphology assessment of the TCBs created in hydrogel-based thin films. This paper is organised as follows. Section 2 will present the analytical mechanical model for the TCBs under small and large deformation conditions, with a particular focus on the estimations of the wavelength and the larger transverse amplitude. In addition, mechanical models will be developed to determine the swelling-induced compressive stress in the hydrogel film and the adhesion toughness between the film and the substrate. Section 3 will examine the mechanical models by using the independent experimental results presented by Takahashi *et al.* [20, 21], and a discussion on the blistering mechanism in hydrogel-based films will also be provided. The concluding remarks will be given in Section 4.

2. Analytical mechanical model for telephone cord blisters

2.1. The Ω-formulae for TCBs under small deformation

Yuan, *et al.* [22] studied the spontaneous formation and morphology parameters of the TCBs in hard thin films under biaxial compressive residual stresses by assuming the existence of a pocket of energy concentration instead of an interface separation of critical size. By applying the Von Kármán geometrically nonlinear mechanics and the interfacial mixed-mode fracture mechanics, completely-analytical formulae, *i.e.*, the Ω-formulae are derived for the two local morphology parameters of TCBs of any shape, that is, width $2R$ and height A_x, and for the two global morphology parameters of TCBs of sinusoidal shape, that is, the wavelength λ and transverse amplitude A_y, as schematically shown in Figure 1. To help readers understanding the present development of the analytical mechanical model, a brief introduction of the theoretical derivations is thought to be necessary.

As shown in Figure 1, the local half-width R and height A_x for the fully-developed TCBs are respectively given by

$$R = 2h\left[\frac{\pi^2 E\Omega\bar{\Omega}}{12(1-\nu^2)\sigma_0}\right]^{1/2} \tag{1}$$

and

$$A_x = \frac{4h\Omega^{1/2}\bar{\Omega}}{\sqrt{3}}\,, \tag{2}$$

where Ω and $\bar{\Omega}$ are expressed as

$$\Omega = \frac{h(1-\nu^2)\sigma_0^2}{2EG_c} = \frac{(1-\nu^2)\sigma_0\varphi_0}{2E} \;\text{ and }\; \bar{\Omega} = 1 + \left(1 - \frac{3}{2\Omega}\right)^{1/2} \tag{3}$$

with h, E, and ν being the thickness, Young's modulus and Poisson's ratio of the thin film, respectively; σ_0 represents the compressive residual stress before the interface delamination occurs, and G_c represents the interface adhesion toughness between the film

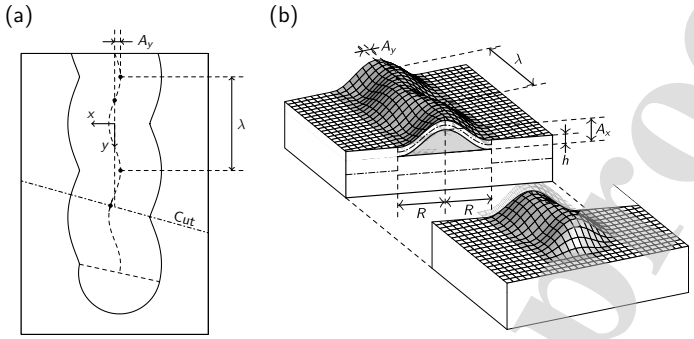

Figure 1: A telephone cord blister of sinusoidal shape. (a): Top view. (b): 3D view of a cut which is perpendicular to the sinusoidal centreline of the TCB.

and the substrate, and $\varphi_0 = h\sigma_0/G_c$. It is seen from Eq. (3) that parameter Ω indicates the ratio between the plane-strain energy density within the thin film before the interface delaminates and the interface adhesion toughness.

The global wavelength λ and transverse amplitude A_y as shown in Figure 1 are respectively given by

$$\lambda = 2R\left(\frac{1-\nu\bar{\Omega}}{\bar{\Omega}-1}\right)^{1/2} \tag{4}$$

and

$$A_y = \frac{\lambda}{\pi}(\bar{A}_y - 1)^{1/2}, \tag{5}$$

with

$$1 + 3\Omega\bar{\Omega}^2 + 2\bar{A}_y^2[\bar{A}_y^2 - 2\Omega\bar{\Omega}(2\bar{A}_y - 1)] = 0\,. \tag{6}$$

It is seen that the analytical Eqs. (1) to (5) derived for the four morphology parameters are determined by the unique parameter Ω; therefore, they are together called 'Ω-formulae' in Ref [22] and current work. Note that the Ω-formulae are only fitting to the TCBs in hard thin films, under the condition of small deformation, exhibiting small transverse amplitude-to-wavelength ratios which are usually less than approximately 1/10. Furthermore, the accuracy of Ω-formulae for predicting the formation, morphology, compressive residual stresses, and interface adhesion toughness have been intensively validated by extensive independent experimental data in Ref. [22]. It is convincingly demonstrated a thin film blistering process driven by the pocket of energy concentration rather than by buckling.

2.2. The Ω-formulae for TCBs under large deformation

As soft hydrogel-based material is highly deformable and flexible, TCBs in hydrogel thin films exhibit very large transverse amplitude-to-wavelength ratios suggesting deep post-secondary-buckling with large geometrical nonlinearity. The Ω-formulae Eqs. (1) and (2) still give accurate predictions for the local width and height; however, Eqs. (4)

to (6) are unable to give accurate predictions for the global wavelength and transverse amplitude for the TCBs under large deformation. It has demonstrated that all four morphology parameters of TCBs are dependent on the parameter Ω. Therefore, empirical formulae are developed below by further correcting Eqs.(4) and (5) for the TCBs in the soft hydrogel-based films. By using the wavelength λ from Eq. (4), the corrected wavelength $\tilde{\lambda}$ for TCBs under large deformation is expressed as

$$\tilde{\lambda} = \lambda \Omega \bar{\Omega}^{1/2} . \tag{7}$$

Next, substituting $\tilde{\lambda}$ into Eq. (5) leads to the corresponding A_y, and it is furthermore inserted into following Eq. (8) to obtain the new $\tilde{A}_y$ for the TCBs under large deformation, that is,

$$\tilde{A}_y = A_y \Omega \bar{\Omega} . \tag{8}$$

Now all four morphology parameters for the TCBs in hydrogel-based soft films that exhibit large deformability can be determined.

2.3. Determination of swelling-induced compressive stress and interface adhesion toughness

It will be shown in Section 3 the validity of the developed Ω-formulae for TCBs under large deformation can be accurately examined by the independent experimental data of TCBs in the soft hydrogel-based films presented in Ref. [20, 21]. This motivates the current development of mechanical models to determine the swelling-induced compressive stresses in gel-based thin film, and the adhesion toughness between the film and the substrate by reversing the developed Ω-formulae presented in Sections 2.1 and 2.2 and using the experimental measurements of morphology parameters of TCBs. The detailed derivations are shown as follows.

2.3.1. Determination of swelling-induced compressive stress in gel-based films

Three mechanical models are developed to determine the swelling-induced compressive stress by using the morphology parameters of the fully-developed TCB in soft gel-based thin films.

(1) Use the measurements of TCB local half-width R and height A_x. The parameter Ω is intended to obtain at first, which is derived from Eq. (2), that is,

$$\Omega = 3 \left(\frac{A_x}{8h} + \frac{h}{A_x} \right)^2 . \tag{9}$$

Note that Eq. (9) is identical to Eq. (2) in Ref. [27], which indicates its applicability to both TCBs and circular blisters. Next, by using Ω given by Eq. (9) and the measured R, the swelling-induced compressive stress in the gel-based thin film can be given by Eq. (10) which is derived from Eq. (1):

$$\sigma_0 = \frac{E\pi^2 \Omega \bar{\Omega}}{3(1-\nu^2)} \left(\frac{h}{R} \right)^2 . \tag{10}$$

It is seen that Eq. (10) is insensitive for $\Omega \gg 1.5$. When $\Omega = 1.5$, Eq. (11) is suggested:

$$\sigma_0 = \frac{E\pi^2}{2(1-\nu^2)} \left(\frac{h}{R} \right)^2 . \tag{11}$$

(2) Use the measurements of local width $2R$ and global wavelength $\tilde{\lambda}$. Based on Eqs. (4) and (7), the ratio of wavelength to width satisfies Eq. (12) that is again subjected to the parameter Ω if Poisson's ratio ν is constant, that is,

$$\frac{\tilde{\lambda}}{2R} = \Omega \left[\frac{\bar{\Omega}\left(1 - \nu\bar{\Omega}\right)}{\bar{\Omega} - 1} \right]^{1/2} . \tag{12}$$

(3) If the interface adhesion toughness G_c is known, then Eq. (3) can be inserted into Eq. (9) or (10) or (12) to directly obtain the swelling-induced compressive stress without calculating the Ω values.

2.3.2. Determination of interface adhesion toughness

Four mechanical models are developed to determine the interface adhesion toughness by using the morphology parameters of the fully-developed TCB in soft gel-based thin films.

(1) If the measurement of swelling-induced compressive stress σ_0 before the interface delamination occurs is known, then the measurement of blister height A_x can be used. Insert Eq. (3) into Eq. (9) to obtain the interface adhesion toughness G_c, that is,

$$G_c = \frac{h\sigma_0^2\left(1 - \nu^2\right)}{6E}\left(\frac{A_x}{8h} + \frac{h}{A_x}\right)^{-2} . \tag{13}$$

(2) Use the measurement of σ_0 and local half-width R of fully-developed TCBs. Substituting Eq. (3) into Eq. (10) leads to

$$G_c = \frac{\pi^2 h\left[4\sigma_0\left(R/h\right)^2 - \pi^2 E/\left(1 - \nu^2\right)\right]}{12\left(R/h\right)^4} . \tag{14}$$

It is also seen that Eq. (14) is insensitive for $\Omega \gg 1.5$. When $\Omega = 1.5$, by using Eq. (3) and Eq. (11), the adhesion toughness is calculated as

$$G_c = \frac{h\sigma_0^2\left(1 - \nu^2\right)}{3E} = \frac{h\pi^4 E}{12\left(1 - \nu^2\right)}\left(\frac{h}{R}\right)^4 . \tag{15}$$

(3) Use the measurements of σ_0, and the TCB global wavelength $\tilde{\lambda}$ and local width $2R$, the interface adhesion toughness G_c can be obtained by combining Eqs. (3) and (12).

(4) If the measurement of σ_0 is unknown, Eqs. (9) to (12) presented in Section 2.3.1 can be used initially to determine the σ_0 value. Then, substitute the σ_0 value into the above methods to obtain the interface adhesion toughness G_c.

In general, G_c value obtained by above-mentioned methods is independent of the mixed-mode fracture partition theories. If, however, the mode I and mode II adhesion toughness are specified individually to determine the overall adhesion toughness, then the TCB morphology parameters do depend on the mixed-mode fracture partition theory, as various fracture partition theories will bring about various values, as illustrated in Ref. [22].

3. Experimental validation and discussions

3.1. The validation of Ω-formulae for TCBs under large deformation

The Ω-formulae under large deformation are now validated by using the independent experimental measurements of TCB morphology reported by Takahashi *et al.* [20, 21]. Readers are encouraged to read their work for the experimental details to fabricate robust architectures via selective swelling in hydrogel-based films. Here only key information with respect to the examinations of Ω-formulae are presented.

Takahashi *et al.* [20, 21] prepared silanised glass coverslips and chemically modified with 3-(trimethoxysilyl)propyl methacrylate (TMSPMA) so that it would covalently bond to the polyacrylamide (PAAm)-based hydrogel film cross-linked by N,N'-methylenebis [acrylamide] (MBAA). Note the monomer concentration used in Refs. [20, 21] were about 4 M that is much higher than 0.5–2 M for conventional PAAm gels. Also, as the monomer concentration increases, the cross-link density may also increase due to entanglement. The overall effect of the high monomer concentration and cross-link density is to increase the Young's modulus of the hydrogel film as reported in the original work. For the single-hydrogel-film composite system prepared in Ref. [21], the Young's modulus is $E = 82.7$ kPa, and the Poisson's ratio is $\nu = 0.5$ indicating incompressible gel, and the swelling ratio is $\Lambda = 1.39$, respectively. By using the photolithographic and oxygen plasma etching techniques, selective non-adhesive rectangular regions were produced at the interface. Therefore, when the film/substrate material system was immersed in the large amount of deionised water, two swelling behaviours were observed: one was the confined swelling where the bottom surface of the hydrogel film was restricted by the substrate thanks to the strong adhesion led by covalent bonds generated between the hydrogel and TMSPMA, and the other one is the side-fixed swelling in the non-adhesive regions where non-covalent interactions were formed, and the hydrogel can freely swell in the thickness direction but cannot expand to the adjacent fixed region. As a result, the swelling pressure and the boundary constraints together lead to biaxial compressive stresses in the hydrogel film. Furthermore, straight-sided blisters were initially observed and later transformed to the TCBs with continuous interfacial delamination until reaching equilibrium, which exhibit large transverse amplitude-to-wavelength ratio $\tilde{A}_y/\tilde{\lambda}$.

Takahashi *et al.* [20, 21] regarded the hydrogel as a Neo-Hookean material, and the swelling-induced compressive stress in the hydrogel is suggested as

$$\sigma_0 = \frac{2E}{3}\left(\frac{1}{\Lambda^2} - \Lambda^4\right). \tag{16}$$

where Λ represents the linear swelling ratio. Note that the deformation of the free swollen gel compresses in biaxial directions; therefore, the compressed swelling ratio $1/\Lambda$ has been inserted into Eq. (16). It is considered that the validation of the accuracy and applicability of Eq. (16) would be of significant value. In addition, Takahashi *et al.* [20, 21] consider that the swelling-induced compression drives buckling occur in the hydrogel film due to the pre-prepared non-adhesive region at the interface, which subsequently generates TCBs with the stress relief. There are two stages of blister growth in the buckling-based approach: first, when the size of the non-adhesive region at the interface reaches the buckling requirement, or alternatively the swelling-induced compressive stress is sufficient to trigger buckling, the free-swelling hydrogel starts to

Table 1: Comparison of compressive stress given by Ω-formulae, Neo-Hookean model, and buckling-based approach

Experimental measurements Ref. [21]			Theoretical predictions				
Thickness h (μm)	Width $2R$ (μm)	Height A_x (μm)	Ω	Compressive stress σ_0 (kPa)			
				Ω-formulae Eq. (11)	Neo-Hookean Eq. (16)	Buckling-based (straight blister model)	Buckling-based (pinned-circular blister model)
89.68	319.58	253.26	1.500	171.4	177.3	199.43	163.42

bend away from the substrate, forming the blister with energy release rate at the original fixed sides. Second, at a critical size slightly larger than the buckling requirement the energy release rate exceeds the adhesion toughness at the interface and the blister grows till to its equilibrium shape where the energy release rate at the boundaries is smaller than the interface adhesion toughness, and its growth stops. However, as will be demonstrated later by the careful calculations, it is found the original swelling-induced compressive stress before bending out is insufficient to generate the blister. In this circumstance, the authors of current paper argue that the blister growth is driven by an extra energy source, called pocket of energy concentration, in addition to the swelling-induced compressive stress. More specifically, the pocket of energy concentration drives the hydrogel film bend away from the substrate, and its propagation under the condition that non-adhesive areas at the interface are too small to trigger buckling. The blister energy which includes the strain energy and fractured surface energy, is larger than the initial compressive strain energy in the un-delaminated film and it increases until it reaches a maximum at the end of the first stage of the blister growth. Subsequently, the blister energy decreases, and the blister stops growing when the blister energy is balanced with the initial swelling-induced strain energy in the un-delaminated film. The detailed discussion of energy transitions between parts of TCBs can be further found in Ref. [22].

To identify which of above-mentioned mechanisms is capable to assess the TCB morphology under large deformation with good accuracy, the swelling-induced compressive stress in the single-hydrogel-film is therefore estimated as the first validation, by using the average measurement values of local half-width R and height A_x, as shown in Figure 2 in which 'Dist' denotes the measured distance. Based on the Ω-formulae developed in Section 2, the value $\Omega = 1.5$ is initially calculated using Eq. (9). Accordingly, the prediction of swelling-induced compressive stress σ_0 is obtained by substituting the average measurement of R into Eq. (11). In addition, predictions of σ_0 based on the buckling approach for TCBs [13,14], namely, straight and pinned-circular blister models, and that out of Eq. (16) are also calculated, and the results are together recorded in Table 1.

It is seen from Table 1 that the predicted swelling-induced compressive stresses derived from the Ω-formulae and the Neo-Hookean material model are very close to each other; however, large difference is observed comparing with the results out of the buckling approaches. This indicates both Ω-formulae and the Neo-Hookean material model are suitable to estimate the swelling-induced compression for the TCBs in the hydrogel film presented in Ref. [20, 21]. For consistency, the swelling-induced compressive stresses in the hydrogel-based films discussed in this work are evaluated by the Neo-Hookean material model as given by Eq. (16). It is worth mentioning that the interface adhesion toughness G_c between the hydrogel film and the chemically modified glass coverslip can be furthermore obtained by using Eq. (15), that is, 8.52 J/m^2, and the corresponding

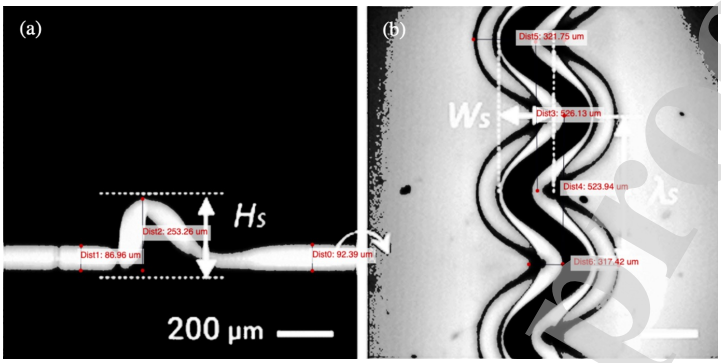

Figure 2: The first TCB under large deformation with morphology measurement. (a): The cross-section view in Grayscale (Dists 0 and 1 are film thickness, Dist 2 is blister height). (b): The top-view in Grayscale (Dists 3 and 4 are wavelength, Dists 5 and 6 are blister width, Coloured version can be found in Figure 2 in Ref. [21]).

Table 2: Comparison of the morphology parameters of the second TCB under large deformation

Experimental measurements Ref. [21]			Theoretical predictions			
Width $2R\,(\mu m)$	Wavelength $\tilde{\lambda}\,(\mu m)$	Transverse amplitude $\tilde{A}_y\,(\mu m)$	Ω	Thickness $h\,(\mu m)$	Height $A_x\,(\mu m)$	Transverse amplitude $\tilde{A}_y\,(\mu m)$
307.24	582.88	133.38	1.722	70.22	289.09	134.92

φ_0 is 1.8660. And note that the equations to determine the wavelength $\tilde{\lambda}$ and transverse amplitude $\tilde{A}_y$ as demonstrated in Section 2 are not applicable because $\Omega = 1.5$; however, their ratio can be obtained as $\tilde{A}_y/\tilde{\lambda} = 0.1395$.

The following examinations are on the prediction accuracy of the TCB morphology parameters through the developed Ω-formulae. As shown in Figure 3, the second hydrogel TCB under large deformation is considered. The average measurement values of local width $2R$ and global wavelength $\tilde{\lambda}$ are substituted into Eq. (12) to obtain the Ω value. Then, together with the compressive stress $\sigma_0 = 177.3$ kPa given by Eq. (16), the resultant thickness of the swollen hydrogel film h is calculated. Next, the height A_x and the transverse amplitude $\tilde{A}_y$ are respectively obtained by using Eq. (2) and Eqs. (5) to (8). The experimental and prediction results are summarized in Table 2.

The prediction of transverse amplitude $\tilde{A}_y$ from the developed Ω-formulae, as shown in Table 2, reaches an excellent agreement with the measured value. It is therefore deduced that the corresponding predictions of the resultant thickness for the swollen hydrogel and the TCB height are reasonably accurate since they are correlated strictly with the unique parameter Ω. Furthermore, the interface adhesion toughness is estimated as 5.81 J/m^2, which is smaller than that illustrated in the first validation. The reason may be the thickness reduction of the hydrogel film. And the corresponding φ_0 is 2.1416.

In the third exercise, the developed Ω-formulae are examined by the TCB with the measurements of local height and global wavelength, $A_x = 320\,\mu m$ and $\tilde{\lambda} = 570\,\mu m$,

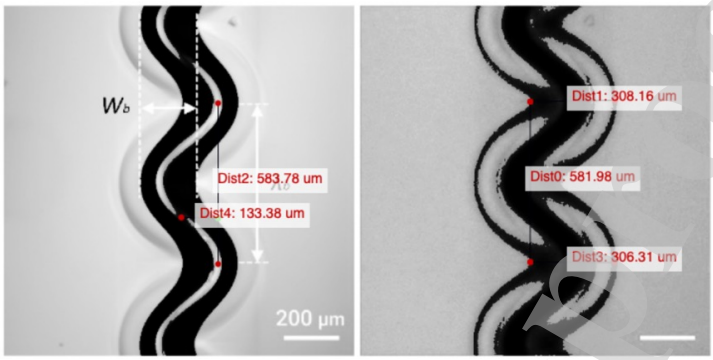

Figure 3: The second TCB under large deformation with morphology measurement. (a): Digital image correlation image (Dist 2 is wavelength, Dist 4 is transverse amplitude). (b) Fluorescent image in Grayscale (Dist 0 is wavelength, Dists 1 and 3 are blister width, Coloured version can be found in Figure S5 in Ref. [21]).

Table 3: Comparison of the morphology parameters of the third TCB under large deformation

Experimental measurements Ref. [21]		Theoretical predictions			
Height A_x (μm)	Wavelength $\tilde{\lambda}$ (μm)	Ω	Thickness h (μm)	Width $2R$ (μm)	Transverse amplitude $\tilde{A}_y$ (μm)
320	570	1.9416	67.33	326.20	164.16

respectively. Again, the swelling-induced compressive stress in the hydrogel film is $\sigma_0 = 177.3$ kPa. It is therefore noted that Eqs. (9), (10) and (12) can be combined to solve the unknown parameters: Ω, h, and R. Then, the prediction of transverse amplitude $\tilde{A}_y$ is obtained by using Eqs. (5) to (8). The results are recorded in Table 3.

Since the experimental measurements of the local width and the global transverse amplitude for the TCB are not available, the accuracy of the predictions from the Ω-formulae for the third TCB is hard to conclude. Nevertheless, it is noted that the adhesion toughness between the hydrogel film and the chemically modified glass coverslip is 4.94 J/m^2 and the corresponding φ_0 is 2.4154, which are close to the values for the second TCB shown in Figure 2. Particularly, the resultant thickness values of the hydrogel films after swelling are close. Under the condition of same swelling-induced compressive stress, it is furthermore deduced the TCB geometries outlined in Tables2 and 3 are analogous to each other. And the morphology parameters of the two hydrogel-film/glass-substrate systems must be comparable. Therefore, by cross-validating the experimental results and theoretical predictions in Tables 2 and 3, it is concluded that estimations from the developed Ω-formulae for the third TCB are of good accuracy.

Now the experimental results presented in Ref. [20] are used to examine the developed Ω-formulae. Two kinds of fluorescein *o*-acrylate (FL) labelled PAAm-based hydrogels were chemically fabricated on the TMSPMA modified coverslip substrates. They were

Table 4: Comparison of the morphology parameters of the series of TCBs under large deformation

Experimental measurements Ref. [20]			Theoretical predictions					
NaCl concentration or Temperature	Height A_x (μm)	'Amplitude' $2A_y$ (μm)	Ω	φ_0	Adhesion toughness G_c (J/m^2)	Width $2R$ (μm)	Wavelength $\tilde{\lambda}$ (μm)	'Amplitude' $2\tilde{A}_y$ (μm)
(a) Ionic strength responsiveness – Poly (SA-co-FL-co-AAm)								
0 mM	424.95	376.57	1.8446	1.7539	18.30	384.6	688.07	363.16
5 mM	383.62	338.18	1.7033	1.6196	19.82	358.2	688.82	311.85
10 mM	377.44	327.77	1.6847	1.6019	20.04	354.34	692.20	306.04
20 mM	349.13	307.27	1.6087	1.5297	20.99	336.88	725.75	287.05
50 mM	344.9	279.61	1.5988	1.5202	21.12	334.32	734.28	285.51
100 mM	336.44	268.22	1.5801	1.5024	21.37	329.22	755.35	283.77
(b) Control hydrogel architectures in a – Poly (FL-co-AAm)								
0 mM	340.67	281.24	1.5892	1.5111	21.24	331.76	744.08	284.41
5 mM	343.60	282.86	1.5958	1.5174	21.16	333.52	737.15	285.13
10 mM	343.28	275.05	1.5950	1.5167	21.17	333.32	737.87	285.04
20 mM	348.48	273.10	1.6072	1.5282	21.01	336.48	726.99	286.79
50 mM	344.25	275.70	1.5973	1.5188	21.14	333.92	735.70	285.32
100 mM	341.97	274.73	1.5921	1.5139	21.21	332.54	740.92	284.70
(c) Thermo-responsiveness – Poly (NIPAM-co-FL-co-AAm)								
25 °C	388.87	337.43	1.7196	1.6351	19.63	361.5	686.76	317.20
30 °C	388.31	327.64	1.7179	1.6334	19.65	361.16	686.95	316.61
35 °C	357.65	298.30	1.6299	1.5498	20.71	342.08	711.84	291.28
(d) Control hydrogel architectures in c – Poly (Fl-co-AAm)								
25 °C	339.17	269.66	1.5859	1.5080	21.29	330.86	747.90	284.13
30 °C	335.11	271.76	1.5773	1.4998	21.40	328.42	759.22	283.68
35 °C	346.45	275.95	1.6024	1.5236	21.07	335.26	731.02	286.03
40 °C	347.99	280.14	1.6060	1.5271	21.02	336.18	727.93	286.60
45 °C	343.23	287.13	1.5950	1.5166	21.17	333.3	737.99	285.02
50 °C	341.27	277.35	1.5906	1.5124	21.23	332.12	742.61	284.54

functionalised by sodium acrylate (SA) to add ionic strength responsiveness and by N-isopropylacrylamide (NIPAM) to add thermo-responsiveness, respectively. It has been experimentally illustrated that the existence of FL in the PAAm polymer backbone does not affect the swelling ratio, mechanical properties such as the Young's modulus, and the morphology of 3D architectures in the hydrogel-based thin film. Next, the hydrogels were immersed in the deionised water for 24 h, and it was observed that TCBs of large $\tilde{A}_y/\tilde{\lambda}$ ratios were generated spontaneously due to swelling, as shown in Figure 4. For the hydrogel with 0.3 mol % cross-linking density, the Young's modulus and Poisson's ratio of are $E = 121$ kPa and $\nu = 0.5$, respectively. And the hydrogel film thickness after swelling is $h = 94.6\,\mu$m with the swelling ratio $\Lambda = 1.47$ determined from the experiment. Therefore, the biaxial compressive stress induced by swelling is calculated as 339.34 kPa based on Eq. (16).

By using the measurements of TCB height A_x provided from Ref. [20] and Eq. (9), the Ω values for the prepared single-hydrogel-film/glass-coverslip systems are determined. Then the corresponding interface adhesion toughness G_c and φ_0 are obtained based on Eqs. (3) and (14). Furthermore, the TCB local half-width R and 'amplitude', as defined in Ref. [20] $2\tilde{A}_y$ are respectively given by Eqs. (1) and Eqs. (5) to (8). All the theoretical predictions are shown in Table 4.

It is seen from Table 4 that the predicted 'amplitudes' are very close to the experimental measurements, which means the developed Ω-formulae for the two global morphology parameters of TCBs under large deformation again work well. Note that the φ_0 values

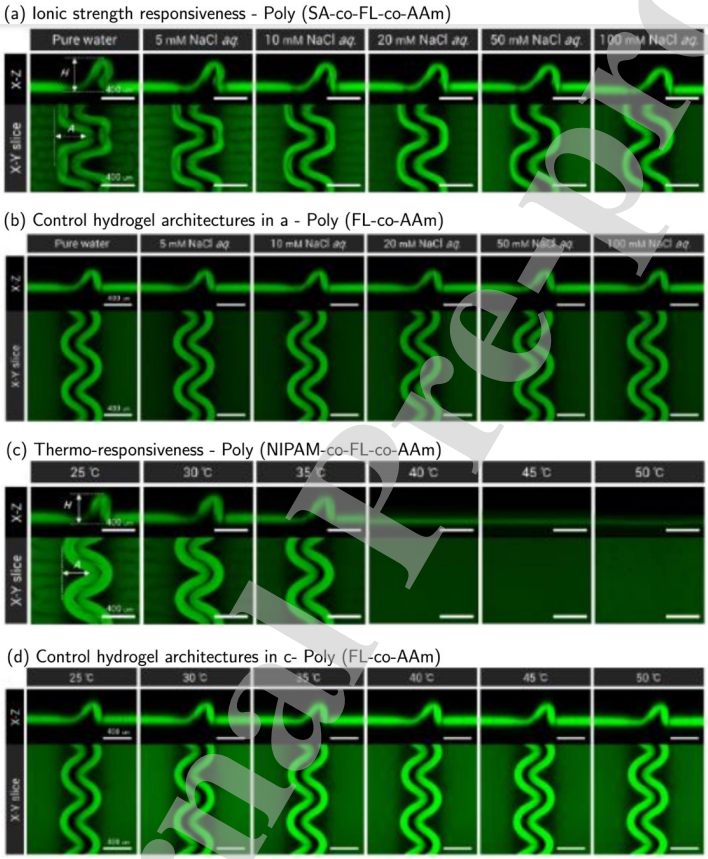

Figure 4: Dynamic control of the series TCBs under large deformation via stimuli-responsive hydrogel films originally presented in Ref. [20].

are extremely small, together with those in the above-mentioned exercises, it is considered small φ_0 value is one of the conditions for TCBs with large $\tilde{A}_y/\tilde{\lambda}$ to form. In addition, the determined G_c values for each group are consistent with each other and reasonable for the non-covalent interactions between the gel film and the glass substrate, which indicates a robust predictive capability for the developed Ω-formulae.

3.2. Discussions on TCB global morphology under small and large deformation

The global wavelength λ and transverse amplitude A_y for TCBs under small deformation are given by Eq. (4) and Eqs. (5) to (6), respectively. For the TCBs under large deformation, the global wavelength $\tilde{\lambda}$ and transverse amplitude $\tilde{A}_y$ are given in the developed Eq. (7) and Eqs. (5) to (8). In contrast, the two local morphology parameters, *i.e.*, width $2R$ and height A_x are expressed in identical formulae. To probe into the conditions for large deformation to occur and its consequences the two global morphology parameters are further studied by comparisons between the small and large deformation scenarios.

The first comparison is made in Figure 5 showing the trends of wavelength-to-width ratio against the height-to-thickness ratio of TCBs. The morphology parameters are extracted from the TCBs in the hydrogel-film/glass-substrate systems used by Takahashi *et al.* [20, 21]; therefore, the Poisson's ratio $\nu = 0.5$ is used in Figure 5. For the same A_x/h and swelling-induced compressive stress σ_0, it is obvious that $\tilde{\lambda}$ under large deformation given by Eq. (12) is larger than λ under small deformation given by Eq. (4). Along with the reduction of the film thickness, or equivalently the increase of A_x/h or Ω, the $\tilde{\lambda}/(2R)$ ratio initially decreases to its minimum value $\tilde{\lambda}/(2R) = 1.71$ with $A_x/h = 5.46$ ($\Omega = 2.25$), and then it increases to monotonically with respect to increases of A_x/h. However, the $\lambda/(2R)$ ratio under small deformation decreases monotonically over the range of A_x/h. This comparison suggests that one possible condition for large deformation to occur is the width $2R$ is small, that is, the TCB is narrow.

In the second comparison, the trends of transverse amplitude-to-wavelength ratio in terms of the parameter Ω are presented, as shown in Figure 6. Along with the increase of Ω, a narrow band of A_y/λ for the TCB under small deformation is observed, with the upper and lower limits as $A_y/\lambda = 0.1053$ ($\Omega \gg 1.5$) and $A_y/\lambda = 0.0930$ ($\Omega = 1.5$), respectively. However, for the TCB under large deformation, the $\tilde{A}_y/\tilde{\lambda}$ ratio monotonically increases from the starting value $\tilde{A}_y/\tilde{\lambda} = 0.1395$ with $\Omega = 1.5$. Therefore, it is reasonable to expect that a certain value of the ratio blister branching can occur to form web blisters which often have large transverse amplitude. Moreover, it is seen that the experimental data from Ref. [20, 21] fall on the predicted $\tilde{A}_y/\tilde{\lambda}$ line generated by Eqs. (5) to (8) nicely. Based on Figures 5 and 6, it is again concluded that the developed Ω-formulae under large deformation are able to provide good predictions of the global transverse amplitude $\tilde{A}_y$ and wavelength $\tilde{\lambda}$ for the TCBs in soft hydrogel-based films.

3.3. Discussions on blistering mechanism for TCBs in soft hydrogel film

Takahashi *et al.* [20, 21] reported intriguing experimental observations of the TCBs created in the hydrogel-based film. Several points are worthy of discussion based on the developed Ω-formulae:

(1) It is experimentally discovered that the blister height increases with increasing the non-adhesive width. As shown by Eq. (2) the increase of blister height corresponds

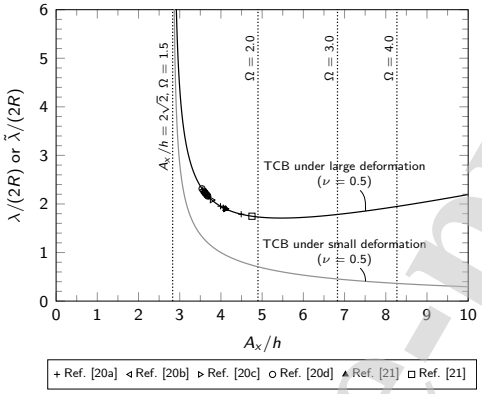

Figure 5: Comparison of wavelength-to-width ratio against height-to-thickness ratio for TCBs under small and large deformation, 'a-c' in the legend denote the four groups of specimens shown in Table 4.

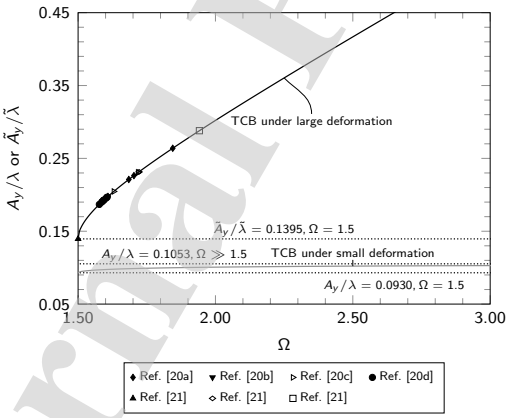

Figure 6: Comparison of transverse amplitude-to-wavelength ratio against the parameter Ω for TCBs under small and large deformation, 'a-c' in the legend denote the four groups of specimens shown in Table 4.

to the increase of parameter Ω, which is further inversely proportional to the interface adhesion toughness G_c. Before the hydrogel film bends away from the substrate, under the condition that the non-adhesive width is smaller than the critical buckling size, the subsequent blister growth and propagation are driven by the pocket of energy concentration. The blister energy which includes the strain energy and G_c, is larger than the initial compressive strain energy due to swelling in the un-delaminated film. However, if the non-adhesive width is larger than the critical buckling value before bending out, buckling will occur and the swelling-induced compressive stress become the driving force, and G_c is not involved if no further interface delamination occurs [13,14].

(2) The blister height also decreases with increasing the cross-linking density, and TCBs were not observed for the cross-linking density values larger than 0.3 mol %. Based on the experimental measurements provided by Takahashi *et al.* [20], the decrease of cross-linking density leads the Young's modulus to decrease while the swelling ratio and the resultant thickness of swollen hydrogel film to increase. Substituting Eq. (16) into Eq. (3) results in

$$\Omega = \frac{2hE(1-\nu^2)}{9G_c}\left(\frac{1}{\Lambda^2} - \Lambda^4\right)^2. \tag{17}$$

Then, by inserting the experimental measurements of Young's modulus and swelling ratio, the average interface adhesion toughness $G_c = 20.75\,\mathrm{J/m^2}$ given from Table 4 into Eqs. (2) and (17), the trend of blister height with respect to the cross-linking density is obtained as shown in Figure 7. It is observed that the blister height increases initially and decreases throughout the cross-linking density, which is in agreement with the experimental observations. Note that the points for the cross-linking density values larger than 0.3 mol % are not included as the corresponding values of Ω is less than 1.5 that is not satisfied by Eq. (3), hence the developed Ω-formulae are not applicable, and no TCBs are expected to form with very small non-adhesive width. More importantly, the condition for the formation of TCBs, that is, $\Omega \geq 1.5$ can be used to determine the critical cross-linking density, and the associated critical swelling ratio of the gel-based material as given by Eq. (17). In contrast, the generation of TCBs with the cross-linking density larger than 0.3 mol % could be led by the large non-adhesive width up to 1000 μm as reported Takahashi *et al.* [20], where TCBs are not driven by the pocket of energy concentration but by buckling.

(3) It is experimentally observed that the deformability of the hydrogel TCBs is increased with increasing the architecture height. This phenomenon can be easily interpreted by Figure 6, where the deformability is represented by the ratios involved global morphology parameter that increases with increasing the value of Ω, or alternatively increasing the blister height as shown by Eq. (2).

(4) The eventual 3D architectures in equilibrium are in the similar shape if the ratios of the non-adhesive width and the initial thickness of hydrogel are similar. This experimental observation indicates the morphology parameters of TCBs in the hydrogel film are determined by the unique parameter Ω. As shown in Eq. (17), in spite of various initial thickness of hydrogel film and small non-adhesive width, the similar Ω values can still be obtained since it is determined by the Young's modulus, Poisson's ratio, thickness of swollen film, and interface adhesion toughness, which are all further related with the cross-linking density. The current work quantitatively correlates the swelling-induced 3D morphological architecture with mechanical properties and compositions of hydrogel

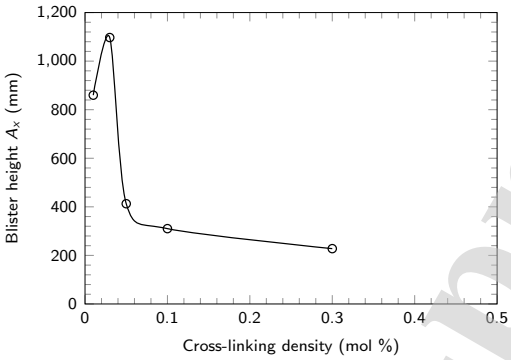

Figure 7: Trend of blister height with respect to cross-linking density using the experimental measurements presented in Ref. [20].

films. This will guide the development of alignment strategy of anisotropic soft additions for soft composites systems that exhibit inhomogeneous swelling. And complex shape-mode could be shifted and synthesised by basic self-bending, -rolling and -twisting, which is beneficial to the design of the microfluidic devices and hydrogel machines [28].

4. Conclusions

Based on a previously developed theoretical framework [18], the 'Ω-formulae' are developed for the telephone cord blisters exhibiting large deformability created in a soft hydrogel-based thin film on a rigid substrate. And the theoretical methods as experimental guidance are proposed for the determination of the swelling-induced compressive stress in the un-delaminated film and the adhesion toughness at the interface. They give accurate predictions of the local half-width and height, and the global wavelength and transverse amplitude; and accurate predictions of the swelling-induced compressive stress that is very close to the value given by the Neo-Hookean model, and consistent value of interface adhesion toughness for the specific film/substrate materials systems. It is suggested that the morphology parameters of 3D architectures created in hydrogel-based films are dependent on the parameter Ω, and most importantly, $\Omega \geq 1.5$ can also be used as the critical conditions for the formation and development of telephone cord blisters with large deformability, which can be further correlated to the critical cross-linking density, swelling ratio, *etc.* For a range of applications in the fields of Tissue Engineering and Bioengineering, the theoretical understanding of the critical condition and post-instability surface evolution could facilitate the development of controllable surface patterns in soft materials. Furthermore, the current work opens the possibilities to design the microfluidic systems by controlling the hollow morphology parameters with high precision, such as modifying the hydrogel composition, swelling ratio, film thickness, and interfacial adhesion toughness.

5. Data availability

The authors confirm that the data supporting the findings of this study are available within the article.

6. Declaration of interests

The authors declare that they have no known competing financial interests or personal relationships that could have appeared to influence the work reported in this paper.

References

[1] B. Yuan, C. M. Harvey, R. C. Thomson, G. W. Critchlow, D. Rickerby, S. Wang, A new spallation mechanism of thermal barrier coatings and a generalized mechanical model, Composite Structures 227 (2019) 111314. doi:10.1016/j.compstruct.2019.111314.

[2] A. Evans, D. Clarke, C. Levi, The influence of oxides on the performance of advanced gas turbines, Journal of the European Ceramic Society 28 (7) (2008) 1405–1419. doi:10.1016/j.jeurceramsoc.2007.12.023.

[3] B. V. Slaughter, S. S. Khurshid, O. Z. Fisher, A. Khademhosseini, N. A. Peppas, Hydrogels in Regenerative Medicine, Advanced Materials 21 (32-33) (2009) 3307–3329. doi:10.1002/adma.200802106.

[4] K. Y. Lee, D. J. Mooney, Alginate: Properties and biomedical applications, Progress in Polymer Science 37 (1) (2012) 106–126. doi:10.1016/j.progpolymsci.2011.06.003.

[5] M. Ilami, H. Bagheri, R. Ahmed, E. O. Skowronek, H. Marvi, Materials, Actuators, and Sensors for Soft Bioinspired Robots, Advanced Materials 33 (19) (2021) 2003139. doi:10.1002/adma.202003139.

[6] Z. Liu, W. Toh, T. Y. Ng, Advances in Mechanics of Soft Materials: A Review of Large Deformation Behavior of Hydrogels, International Journal of Applied Mechanics 07 (05) (2015) 1530001. doi:10.1142/s1758825115300011.

[7] J. Abdolahi, M. Baghani, N. Arbabi, H. Mazaheri, Finite bending of a temperature-sensitive hydrogel tri-layer: An analytical and finite element analysis, Composite Structures 164 (2017) 219–228. doi:10.1016/j.compstruct.2016.12.063.

[8] A. S. Gladman, E. A. Matsumoto, R. G. Nuzzo, L. Mahadevan, J. A. Lewis, Biomimetic 4D printing, Nature Materials 15 (4) (2016) 413–418. doi:10.1038/nmat4544.

[9] A. Drozdov, J. d. Christiansen, Swelling-induced bending of bilayer gel beams, Composite Structures 153 (2016) 961–971. doi:10.1016/j.compstruct.2016.06.076.

[10] Z. Zhou, Z. He, S. Yin, X. Xie, W. Yuan, Adhesive, stretchable and antibacterial hydrogel with external/self-power for flexible sensitive sensor used as human motion detection, Composites Part B: Engineering 220 (2021) 108984. doi:10.1016/j.compositesb.2021.108984.

[11] A. Evans, D. Mumm, J. Hutchinson, G. Meier, F. Pettit, Mechanisms controlling the durability of thermal barrier coatings, Progress in Materials Science 46 (5) (2001) 505–553. doi:10.1016/s0079-6425(00)00020-7.

[12] C. M. Stafford, C. Harrison, K. L. Beers, A. Karim, E. J. Amis, M. R. VanLandingham, H.-C. Kim, W. Volksen, R. D. Miller, E. E. Simonyi, A buckling-based metrology for measuring the elastic moduli of polymeric thin films, Nature Materials 3 (8) (2004) nmat1175. doi:10.1038/nmat1175.

[13] Z. Nie, E. Kumacheva, Patterning surfaces with functional polymers, Nature Materials 7 (4) (2008) 277–290. doi:10.1038/nmat2109.

[14] B. Li, Y.-P. Cao, X.-Q. Feng, H. Gao, Mechanics of morphological instabilities and surface wrinkling in soft materials: a review, Soft Matter 8 (21) (2012) 5728–5745. doi:10.1039/c2sm00011c.

[15] J. Dervaux, M. B. Amar, Mechanical Instabilities of Gels, Annual Review of Condensed Matter Physics 3 (1) (2012) 311–332. doi:10.1146/annurev-conmatphys-062910-140436.

[16] W. Tang, S. Zhu, D. Jiang, L. Zhu, J. Yang, N. Xiang, Channel innovations for inertial microfluidics, Lab on a Chip 20 (19) (2020) 3485–3502. doi:10.1039/d0lc00714e.

[17] M. Moon, H. Jensen, J. Hutchinson, K. Oh, A. Evans, The characterization of telephone cord buckling of compressed thin films on substrates, Journal of the Mechanics and Physics of Solids 50 (11) (2002) 2355–2377. doi:10.1016/S0022-5096(02)00034-0.

[18] J. W. Hutchinson, Z. Suo, Mixed mode cracking in layered materials, Advances in applied mechanics 29 (1991) 63–191.

[19] S. Edmondson, K. Frieda, J. Comrie, P. Onck, W. Huck, Buckling in Quasi-2D Polymers, Advanced Materials 18 (6) (2006) 724–728. doi:10.1002/adma.200501509.

[20] R. Takahashi, H. Miyazako, A. Tanaka, Y. Ueno, Dynamic Creation of 3D Hydrogel Architectures via Selective Swelling Programmed by Interfacial Bonding, ACS Applied Materials & Interfaces 11 (31) (2019) 28267–28277. doi:10.1021/acsami.9b05552.

[21] R. Takahashi, H. Miyazako, A. Tanaka, Y. Ueno, M. Yamaguchi, Tough, permeable and biocompatible microfluidic devices formed through the buckling delamination of soft hydrogel films, Lab on a Chip 21 (7) (2021) 1307–1317. doi:10.1039/d0lc01275k.

[22] B. Yuan, C. M. Harvey, R. C. Thomson, G. W. Critchlow, D. Rickerby, S. Wang, Spontaneous formation and morphology of telephone cord blisters in thin films: The Ω formulae, Composite Structures 225 (2019) 111108. doi:10.1016/j.compstruct.2019.111108.

[23] C. M. Harvey, B. Wang, S. Wang, Spallation of thin films driven by pockets of energy concentration, Theoretical and Applied Fracture Mechanics 92. doi:10.1016/j.tafmec.2017.04.011.

[24] S. Wang, C. M. Harvey, B. Wang, Room temperature spallation of α-alumina films grown by oxidation, Engineering Fracture Mechanics 178 (2017) 401–415. doi:10.1016/j.engfracmech.2017.03.002.

[25] B. J. Briscoe, S. S. Panesar, The application of the blister test to an elastomeric adhesive, Proceedings of the Royal Society of London. Series A: Mathematical and Physical Sciences 433 (1887) (1991) 23–43. doi:10.1098/rspa.1991.0033.

[26] C. M. Harvey, S. Wang, B. Yuan, R. C. Thomson, G. W. Critchlow, Determination of mode I and II adhesion toughness of monolayer thin films by circular blister tests, Theoretical and Applied Fracture Mechanics 94 (2018) 34–39. doi:10.1016/j.tafmec.2018.01.006.

[27] B. Yuan, C. M. Harvey, G. W. Critchlow, R. C. Thomson, S. Wang, Determination of residual stress and interface adhesion toughness of thin films by blisters, Material Design & Processing Communications 1 (5). doi:10.1002/mdp2.60.

[28] X. Liu, J. Liu, S. Lin, X. Zhao, Hydrogel machines, Materials Today 36 (2020) 102–124. doi:10.1016/j.mattod.2019.12.026.

Author Statement

Bo Yuan: Methodology, Investigation, Formal analysis, Data curation, Writing - Original draft preparation

Christopher M. Harvey: Supervision, Conceptualization, Validation, Writing - Reviewing and Editing

Ke Shen: Resources, Visualization

Rachel Thomson: Supervision

Gary Critchlow: Supervision

David Rickerby: Supervision

Suyuan Yu: Resources, Visualization

Simon Wang: Supervision, Conceptualization, Methodology, Writing - Reviewing and Editing

Declaration of interests

☒ The authors declare that they have no known competing financial interests or personal relationships that could have appeared to influence the work reported in this paper.

☐The authors declare the following financial interests/personal relationships which may be considered as potential competing interests:

none

2021-11-08

Swelling-induced telephone cord blisters in hydrogel films

Yuan, Bo

Elsevier

Yuan B, Harvey CM, Shen K, et al., (2021) Swelling-induced telephone cord blisters in hydrogel films. Composite Structures, Volume 280, January 2022, Article number 114909
https://doi.org/10.1016/j.compstruct.2021.114909